Impedance and electric modulus study of amorphous TiTaO thin films: highlight of the interphase effect

Ahlem Rouahi, Abdelkader Kahouli, Fatiha Challali, Marie-Paule Besland, Corentin Vallée, Béchir Yangui, Siamak Salimy, Antoine Goullet, Alain Sylvestre

Impedance and electric modulus study of amorphous TiTaO thin films: highlight of the interphase effect

A Rouahi[1,2], A Kahouli[1,2], F Challali[3], M P Besland[4], C Vallée[5], B Yangui[2], S Salimy[4], A Goullet[4] and A Sylvestre[1]

1 Grenoble Electrical Engineering Laboratory (G2ELab), CNRS, University of Grenoble (UJF), 25 Rue de Martyrs, BP166, 38042 Grenoble CEDEX 9, France
2 Laboratory of Materials, Organization and Properties (LMOP), Campus Universities, El Manar, 2092 Tunis, Tunisia
3 Laboratoire des Sciences des Procédés et des Matériaux (LSPM)-CNRS-UPR3407, Université Paris13, 99 Avenue Jean-Baptiste Clément, 93430, Villetaneuse, France
4 Institut des Matériaux Jean Rouxel – IMN – UMR CNRS 6502, Université de Nantes, 2, rue de la Houssinière, B.P. 32229, 44322, Nantes Cedex 3, France
5 LTM, CNRS, University of Grenoble (UJF), CEA-LETI, Minatec, 17 avenue des Martyrs, 38054 Grenoble Cedex 9, France

Abstract
The influence of phases and phase's boundaries of TiO_2 and Ta_2O_5 in the dielectric and electric response of TiTaO (100 nm thick) elaborated by RF magnetron sputtering was highlighted by complex impedance spectroscopy. Dielectric and electric modulus properties were studied over a wide frequency range (0.1–10^5 Hz) and at various temperatures (−160 to 120 °C). The diagram of Argand (ε'' versus ε') shows the contribution of phases, phases' boundaries and conductivity effect on the electric response of TiTaO thin films. Moreover, the resistance of the material decreases when the temperature increases, thus the material exhibits a negative temperature coefficient of resistance. The electric modulus plot indicates the presence of two peaks of relaxation. The first relaxation process appears at low temperature with activation energy of about 0.22 eV and it is related to the first ionization energy of oxygen vacancies. The second relaxation process appears at high temperature with activation energy of about 0.44 eV. This second peak is attributed to the Maxwell–Wagner–Sillars relaxation. The plots of the complex dielectric modulus and the impedance as a function of frequency allow concluding to a localized relaxation due to the long-range conductivity in the TiTaO film.

1. Introduction

Metal–insulator–metal (MIM) capacitors are key compounds of electronic circuits and they are widely used for dynamic random access memories (DRAMs) and radio-frequency (RF) applications, themselves stimulated over the last decade by a vertiginous increase of the wireless communications [1–7]. To achieve higher capacitance density, the introduction of high-κ dielectrics is one of the most desirable choices. Numerous conventional oxides such as TiO_2, HfO_2, Ta_2O_5, Y_2O_3, Pr_2O_3, Al_2O_3 and (Ba, Sr) TiO_3 have been investigated for such a purpose [1, 3, 5, 8–11]. In order to improve the properties of pure materials and to overcome the undesired high leakage current generated by these materials, many researchers have focused their works on the mixed phase high-k insulating materials such as CeAlO, TiPrO, SrTaO, HfTiO, TiNiO and TiLaO [2–7, 12–15]. Recently, TiTaO thin films, mainly composed of a mixture of two phases (TiO_2 and Ta_2O_5) [12], were used to overcome the issue of high leakage current without sacrificing the capacitance density. In this context, Chiang *et al* show that amorphous 17 nm thick TiTaO film, deposited at 400 °C by physical vapour deposition on TaN/Ta

bottom, exhibits a high capacitance density of 23 F μm^{-2} with a high-κ value of 39 [15]. In addition, TiTaO MIM capacitors showed lower leakage currents of about 1.2×10^{-6} A cm^{-2}, which are $\sim$ 5–7 orders of magnitude smaller than those of TiO_2 devices [7]. Additionally, in this work, Lukosius *et al* demonstrated that TiTaO films deposited at 400 °C on TiN electrodes and having a ratio of Ti/Ta equal to 1.5 were amorphous with a dielectric constant of 50 and a leakage current density as low as 10^{-7} A cm^{-2} at 1 V [7].

In a former work, x-ray photoelectron spectroscopy (XPS) analysis for TiTaO films deposited by magnetron sputtering on TiN electrodes reveals that the material presents Ta_2O_5 and TiO_2 phases with a mixed compound of Ti–Ta bounds [12]. The presence of phases into materials generates the existence of interfaces which play an important role governing the dielectric properties [10, 16, 17]. When an electric field is applied inside heterogeneous systems which contain different media with dissimilar conductivities and permittivities, interfacial polarization mechanisms take place because of the accumulation of electric charges at the interfaces of these media. This effect is known as Maxwell–Wagner–Sillars (MWS) relaxation. Complex impedance spectroscopy (CIS) constitutes one of the electric techniques of characterization among the most adapted to scrutinize the physical mechanisms inherent in mixture phase materials. CIS is particularly relevant when the dielectric properties of materials are significantly affected by interface effects (such as grain boundaries, pores and interface between phases [8, 18, 19]. For composite materials, this technique enables one to separate the contributions of phases, phase's boundaries and electrode/material interfaces using formalisms as the complex permittivity (ε^*), complex electric modulus (M^*) and complex impedance (Z^*). These formalisms are in relation to the ones with the others as follows:

$$\frac{1}{\varepsilon^*(\omega)} = M^*(\omega) = M'(\omega) + \mathrm{j}M''(\omega), \tag{1}$$

$$Z^*(\omega) = Z'(\omega) - \mathrm{j}Z''(\omega) = \frac{1}{\mathrm{j}\omega C_0 \varepsilon^*(\omega)} \tag{2}$$

with

$$\varepsilon^*(\omega) = \varepsilon'(\omega) - \mathrm{j}\varepsilon''(\omega). \tag{3}$$

In these equations, $\mathrm{j} = \sqrt{-1}$, $\omega = 2\pi f$ is the radial frequency with f the frequency and C_0 is the vacuum capacitance. $\varepsilon'(\omega)$, $M'(\omega)$ and $Z'(\omega)$ denote the real part of permittivity, electric modulus and complex impedance, respectively. $\varepsilon''(\omega)$, $M''(\omega)$ and $Z''(\omega)$ denote the imaginary part of permittivity, electric modulus and complex impedance, respectively. The plotting of $\varepsilon''(\omega)$ versus $\varepsilon'(\omega)$ or $M''(\omega)$ versus $M'(\omega)$ makes it possible to represent a given relaxation mechanism by a single semi-circle. This representation is also valid for a set of many relaxations. In this latter case, various semi-circles are more or less decorrelated in this representation. This formalism will be adopted to analyse some results in this study.

The use of the electric modulus formalism enables one to investigate the MWS polarization which is masked by a strong conductivity effect observed at low frequencies when the conventional complex permittivity formalism is adopted. With the final objective using TiTaO as high-k dielectric for capacitances, it seems necessary to study its dielectric properties starting from the CIS technique.

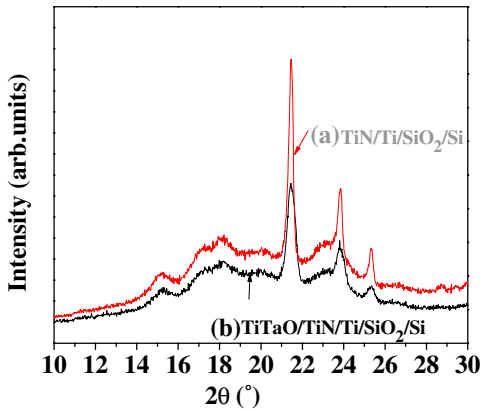

Figure 1. XRD scans of (a) TiTaO/TiN/Ti/SiO_2/Si and (b) TiN/Ti/SiO_2/Si substrates.

In this work, we highlight the interphases (TiO_2/Ta_2O_5) polarization effect on the dielectric response of TiTaO thin films.

2. Experiment

TiTaO thin films (100 nm thick) were deposited on TiN/Ti/SiO_2/Si (1 0 0) substrates by RF magnetron sputtering using a stoichiometric $Ti_{0.6}Ta_{0.4}O$ target. The films were deposited at 350 °C using a power density of 4.45 W cm^{-2} in reactive atmosphere (Ar/O_2) with oxygen content of 20% in the gas phase. The thickness of TiTaO films was determined both by spectroellipsometry and high-resolution transmission electron microscopy (HRTEM). The microstructure of the films was performed by x-ray θ–2θ diffraction (XRD) using Discover D8 x-ray diffractomer (SIEMENS). The measurement of the surface roughness of the material was carried out by atomic force microscopy (AFM) using a tapping mode. For impedance measurements, gold top electrodes were deposited by the Joule effect under vacuum of about 5×10^{-5} Torr to constitute the planar MIM capacitors. Electrical measurements were performed under nitrogen gas to prevent oxidation in the frequency range from 10^{-1} to 10^5 Hz using a Novocontrol BDS20 impedance meter at temperatures ranging from −160 to 120 °C. Temperature was controlled by a Linkam hot-stage TMS94.

3. Results and discussion

3.1. Structural characterization

In order to check the crystallinity of TiTaO thin films, XRD analysis was performed. As can be seen in figure 1, only peaks related to the substrate are detected and we thus conclude here that TiTaO deposited by RF magnetron sputtering at 350 °C has an amorphous structure. Consequently, TiTaO films do not contain grain/grain boundary interfaces as can be seen in many high-k oxides.

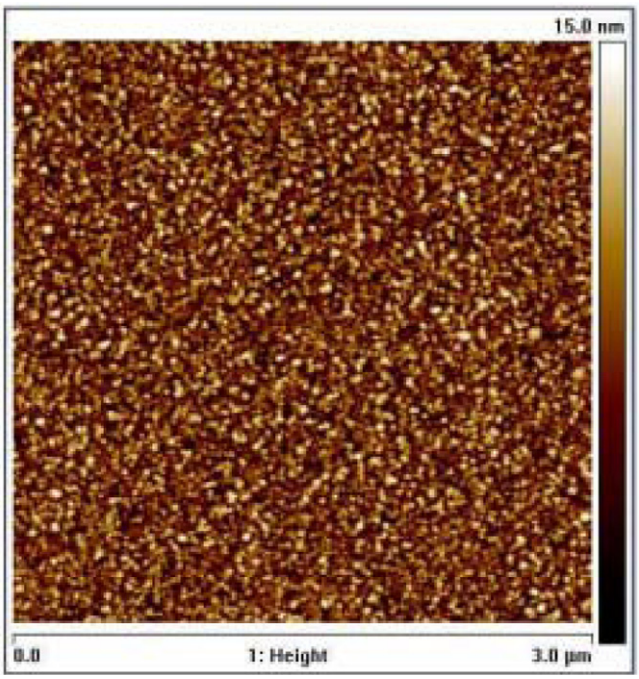

Figure 2. AFM surface morphology of TiTaO thin film (100 nm thick).

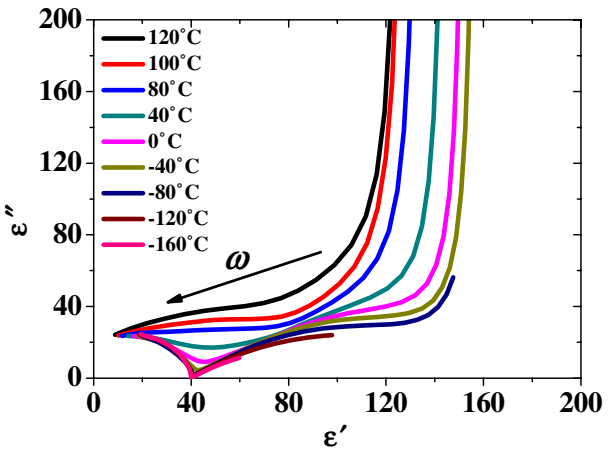

Figure 3. Argand (Cole–Cole) plots at various temperatures.

Figure 2 presents a topographic AFM image over a scan area of 3 μm × 3 μm for a100 nm thick TiTaO thin film. The AFM observation highlights a surface topography exhibiting a homogeneous distribution. Recently, using parallel angle resolved x-ray photoelectron spectroscopy (PARXPS), we demonstrated that TiTaO material is composed of amorphous agglomerates of TiO_2, Ta_2O_5 and a mixed oxide phase with Ti–O–Ta bridging bonds [12]. The root-mean-square (rms) roughness over the scanned areas is about 2.44 nm.

3.2. Impedance analysis

Figure 3 shows the typical real (ε') and imaginary (ε'') parts of the complex permittivity plotted in the complex plane (Cole–Cole diagram) for TiTaO thin films at various temperatures. For temperatures below −80 °C, measurements show clearly the existence of two depressed semicircles. As already said, the existence of several phases into TiTaO was demonstrated by PARXPS [12]. The semicircle at low frequencies can be attributed to the contribution of interphases (phase's boundaries) whereas that at high frequencies can be attributed to phases (bulk effect). The centre of the semicircle is below the abscissa which indicates a non-Debye relaxation illustrating the existence of distributed relaxation times (τ). In this case, the dc conductivity of the material can be neglected and we note that the common point of the two semicircles is at the abscissa $\varepsilon' = 40$. However, to take into account the effect of a distribution of relaxation times, the complex permittivity ε^* can be formally given by the empirical Cole–Cole relaxation [20, 21]:

$$\varepsilon^* = \varepsilon' - \mathrm{j}\varepsilon'' = \varepsilon_\infty + (\varepsilon_S - \varepsilon_\infty)/(1 + (\mathrm{j}\omega\tau)^{1-\alpha}), \quad (4)$$

where ε_S is the static permittivity, ε_∞ is the permittivity at high frequencies and α is a parameter with $0 < \alpha < 1$.

At low frequencies, the plots show that a vertical straight line begins. This line is due to the dc conductivity σ_{dc} effect occurring in the material. Its origin will be discussed further.

Taking into account this dc conductivity, the Cole–Cole equation (equation (4)) can be written as

$$\varepsilon^* = \varepsilon' - \mathrm{j}\varepsilon'' = \varepsilon_\infty + (\varepsilon_S - \varepsilon_\infty)/(1 + (\mathrm{j}\omega\tau)^{1-\alpha}) - \mathrm{j}\frac{\sigma}{\omega}. \quad (5)$$

The common point of the two semicircles at $\varepsilon' = 40$ shifts with the increase in temperature and the second semicircle observed at the lowest frequencies deviates and totally disappears from 100 °C. Indeed, for temperatures higher than this value, the dc conductivity dominates and the material becomes more conductive.

In figure 4(*a*), the real impedance spectra (Z') as a function of frequencies and temperatures is plotted. A decrease in Z' with the increase in temperature at low frequency is seen. This behaviour suggests that the material possesses a negative temperature coefficient of resistance (NTCR) [10, 22, 23]. It is also found that all curves merge into a single curve at high frequencies independently of the temperature, showing the space charge dependent behaviour of the material [10]. Indeed, the charge carriers which are accumulated in the vicinity of the phase's boundaries have sufficient energy to surmount the barrier thus leading to an increase in the conductivity and a reduction in the impedance. The imaginary part of the impedance as a function of frequency and temperature is shown in figure 4(*b*). One observes a single impedance relaxation peak which appears at −60 °C and shifts towards the high frequencies with an increase in temperature. This implies that the electrical relaxation phenomenon of the TiTaO film is thermally activated. This behaviour highlights that the relaxation time of the mobile charge carriers decreases with an increase in temperature. In addition, the maximum value of Z'' decreases quickly with the temperature thus illustrating the strong dependence of the resistance of material with the temperature [18]. The Z'' peaks obey the Arrhenius law (figure 5). From the slope of the linear fit, activation energy of about 0.43 eV is obtained.

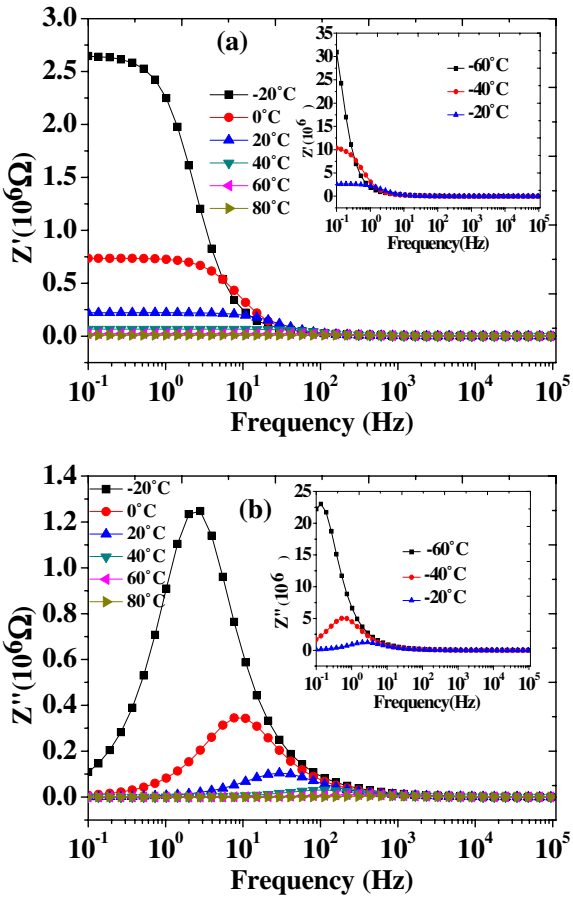

Figure 4. (a) Real part of impedance (Z') and (b) imaginary part of impedance (Z'') as a function of frequency and for various temperatures of measurement. Inset: measurements at the lowest temperatures.

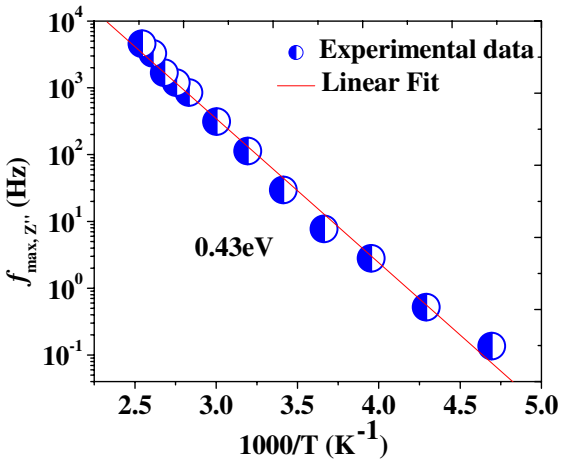

Figure 5. Arrhenius plot of relaxation frequency from impedance spectra.

3.3. Modulus analysis

The complex electric modulus formalism M^* is often used to analyse the space-charge relaxation phenomena, which is not clearly detected when the complex permittivity formalism is used. This approach also highlights the space-charge

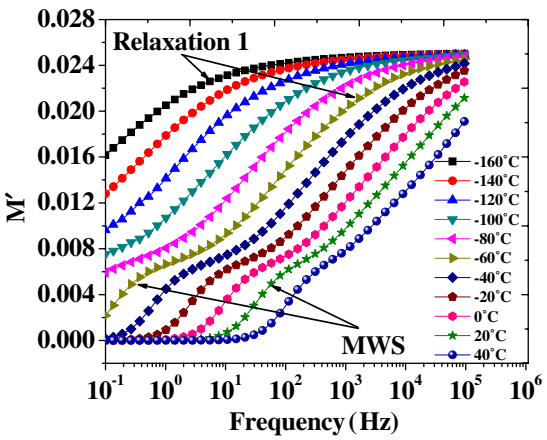

Figure 6. Real part M' of the electric modulus versus frequency of TiTaO thin films at various temperatures.

phenomena with smallest capacitance and it can suppress the contribution of electrode polarization effects [8, 17, 24].

Figure 6 shows the variation of the real part of the complex impedance M' as a function of frequency and temperature. It can be clearly seen that the values of M' increased with the frequency at each temperature, and present a constant value at both high frequencies and low temperatures. Between these plateaus, the polarization effect is evidenced.

Figure 7(a) shows the variation of the imaginary part of the electric modulus (M'') with the frequency at various temperatures. At very low temperature, the spectrum exhibits a first peak of relaxation (relaxation 1) which moves towards higher frequencies when temperature increases. The activation energy (E_a) of this relaxation process was evaluated using the Arrhenius equation $f = f_0 \exp(-E_a/k_b T)$, where f_0 is defined as the pre-exponential factor and k_b is the Boltzmann constant. The value of found energy is 0.22 eV (figure 7(c)) and it is attributed to the first ionization energy of oxygen vacancies and/or the reduction of Ti^{4+} into Ti^{3+} [12, 25, 26]. These mechanisms are expressed by the equations:

$$V_O \rightarrow V_O^{\cdot} + e', \tag{6}$$

$$Ti^{4+} + e' \rightarrow Ti^{3+}. \tag{7}$$

At −60 °C and in the frequency range of our study, a second relaxation peak (relaxation 2) appears at very low frequency. This peak is related to the appearance of the previously discussed straight line of the dc conductivity which is in the same frequency range (figure 3). Low-frequency relaxations are often correlated with interfacial effects [16, 17]. Indeed, in the case of heterogeneous materials containing components with different conductivities and permittivities, the charges accumulate to the interfaces when an electric field is applied (MWS relaxation). The relaxation frequency dependence of this second process as a function of the reciprocal temperature follows the Arrhenius law with activation energy of about 0.44 eV (figure 7(d)) which is the same value found by the extraction made from Z'' spectra. This value is allotted to the MWS relaxation occurring at the interfaces between the phases existing in TiTaO films. Similar behaviours have been observed in other materials such as polymers or oxides [8, 16].

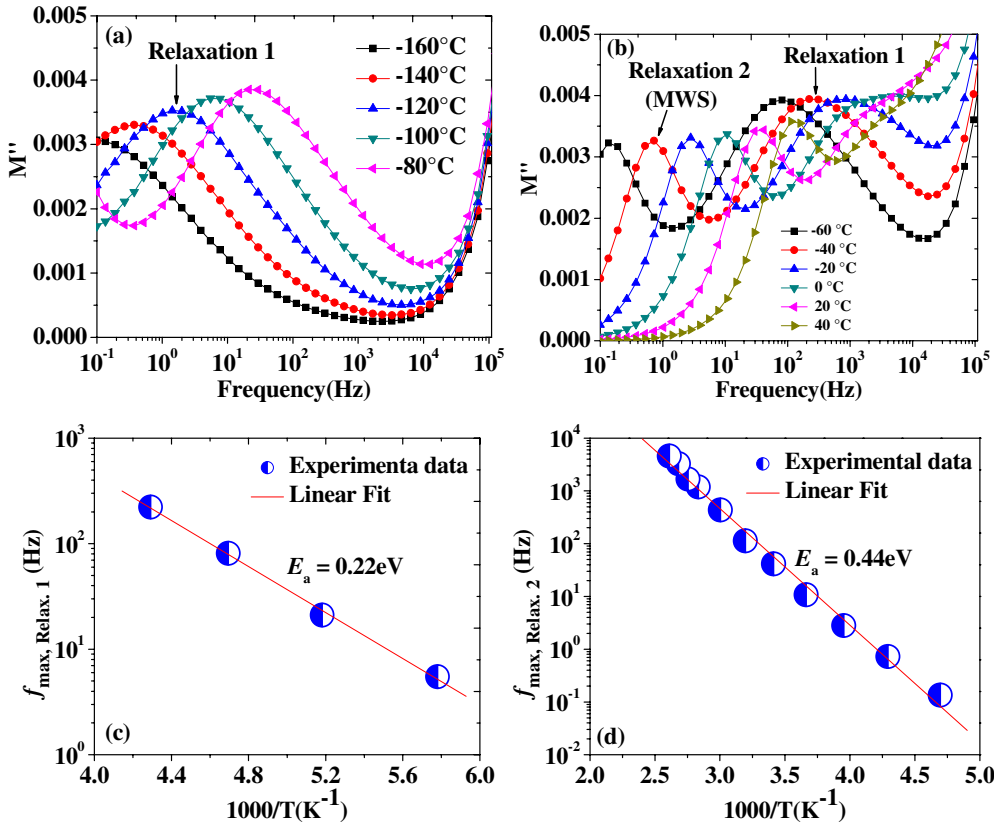

Figure 7. Variation of M'' for temperatures: (a) below $-60\,^{\circ}$C, (b) above $-60\,^{\circ}$C and Arrhenius diagram of (c) first relaxation and (d) second relaxation: MWS.

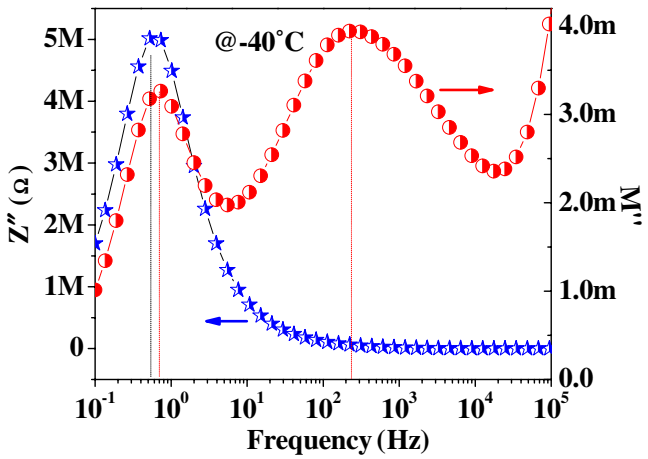

Figure 8. Z'' and M'' plots extracted at $-40\,^{\circ}$C as a function of frequency.

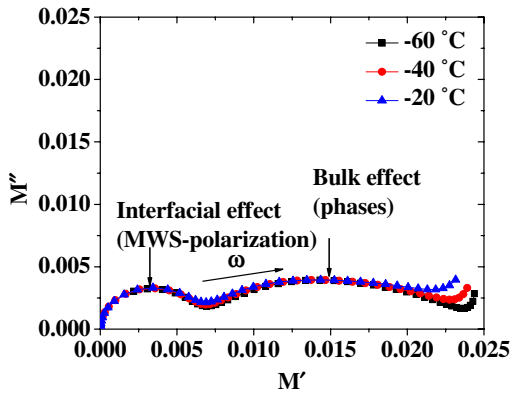

Figure 9. Complex electric modulus plane plot (M'' versus M').

The dependence of Z'' and M'' with the frequency measured at $-40\,^{\circ}$C for TiTaO films is represented in figure 8. Both electric parameters are simultaneously considered in order to separate the localized (short-range conduction associated with the dielectric relaxation) and the non-localized (long-range associated with the dc-conduction) conductions. According to figure 8, the separation of Z'' and M'' peaks shows a localized relaxation due to the long range conductivity in the amorphous TiTaO thin films.

Figure 9 reports the complex plane plot M'' versus M' at various temperatures. A large semicircle at high frequencies is observed and it is attributed to the bulk effect (phase effect), whereas a small semicircle takes place at low frequencies which originates from the phase boundary effect. From this curve, we can deduce that the phase boundaries capacitance is smaller than that of phase [17].

3.4. Electrical conductivity

Figure 10(a) shows the frequency variation of ac conductivity at various temperatures. In the frequency range of our study, the conductivity obeys the Jonscher power law given by the following equation:

$$\sigma_{ac} = \sigma_{dc} + A\omega^n, \tag{8}$$

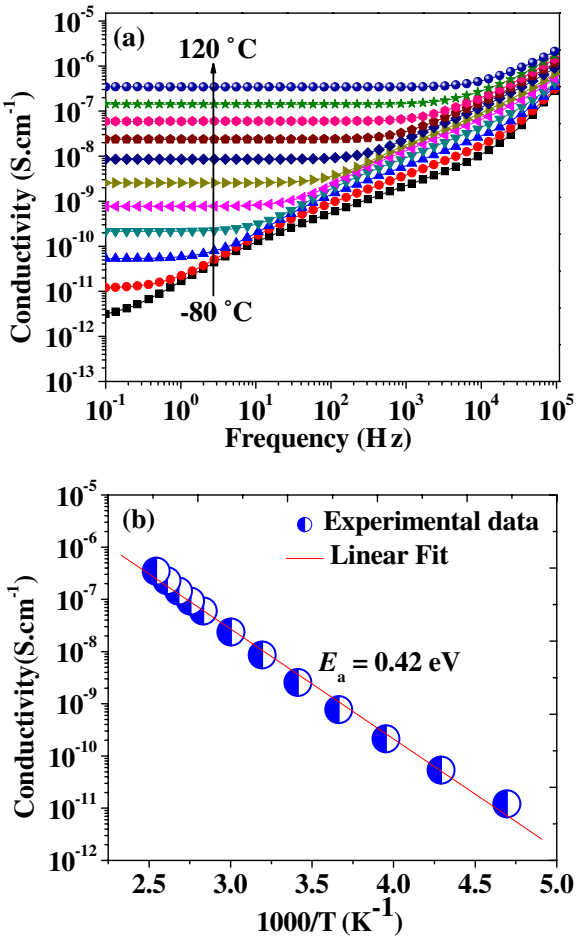

Figure 10. (*a*) Frequency dependence of the ac conductivity at various temperatures with $\Delta T = 20\,^{\circ}$C and (*b*) dc conductivity (σ_{dc}) as a function of $1000/T$.

where σ_{dc} is the frequency-independent conductivity, A is a temperature-dependent factor and n is the frequency exponent ($0 < n < 1$) [18].

The particular frequency where the change in slope of the ac conductivity takes place is known as the critical frequency (ω_c) which is a sign of the change in the conductivity mechanisms from the long range to the short range conduction. One observes that the critical frequency is temperature dependent, and it shifts towards higher frequencies with an increase in temperature. Below this critical frequency, the dc conductivity dominates at high temperature. To identify the main conduction mechanism occurring in the amorphous TiTaO, we plotted σ_{dc} versus the inverse of temperature (figure 10(*b*)). It is clearly seen that σ_{dc} obeys the Arrhenius law with activation energy of about 0.42 eV which is the same value obtained for MWS relaxation. This result suggests that the same charge carriers contribute to the conduction mechanism and the MWS polarization. Dc current–voltage measurements are in progress to confirm this extremely probable assumption.

4. Conclusion

Electric properties of amorphous TiTaO thin films elaborated by RF magnetron sputtering at 350 °C were investigated by complex impedance spectroscopy in large frequency (0.1–10^5 Hz) and temperature (−160 to 120 °C) ranges. Contribution of phases, phase's boundaries and electric conduction are evidenced in the electric response of TiTaO as the frequency decreases. The imaginary modulus shows two peaks of relaxation. The first relaxation process appears at low temperature with activation energy of about 0.22 eV and it is related to the first ionization of oxygen vacancies, while the second relaxation process appears at high temperature with activation energy of about 0.44 eV. This second relaxation process is related to the Maxwell–Wagner–Sillars relaxation. The plot of the electric parameters (M'' and Z'') versus frequency shows that the peaks do not overlap each other, indicating the presence of a localized relaxation of a long-range interaction in the amorphous TiTaO thin films. Finally, the ac conductivity analyses revealed that the same charge carriers seem responsible for the conduction mechanism and the Maxwell–Wagner–Sillars polarization.

Acknowledgment

The first author would like to thank the 'Agence Universitaire de la Francophonie' (AUF) for the financial support of this work.

References

[1] Iternational Roadmap for Semiconductors 2009 *RF and Analog/Mixed-Signal Technologies for Wireless Communications* (Palo Alto, CA: Semiconductors Industry Association)
[2] Baristian Kaynak C, Lukosius M, Costina I, Tillack B, Wenger Ch, Ruhl G and Rushworth S 2010 *Microelectron. Eng.* **87** 2561
[3] Atanasova E, Spassov D, Paskaleva A, Georgieva M and Koprinarova J 2008 *Thin Solid Films* **516** 8684
[4] Huang C, Cheng C-H, Lee K-T and Liou B-H 2009 *J. Electr. Soc.* **156** G23
[5] Cheng C H, Hsu H H, Chen P C, Liou B H, Chin A and Yeh F S 2010 *Solid- State Electron.* **54** 646
[6] Huang C C, Cheng C H, Albert Chin and Chou C P 2007 *Electrochem. Solid-State Lett.* **10** H287
[7] Lukosius M, Baristiran Kaynak C, Wenger Ch, Ruhl G, Rushworth S and Baumann P 2011 *Thin Solid Films* **519** 3831
[8] Martinez R, Kumar A, Palai R, Scott J F and Katiyar R S 2011 *J. Phys. D: Appl. Phys.* **44** 105302
[9] Liu G-Z *et al* 2008 *Appl. Phys. Lett.* **92** 122903
[10] Barik S K, Choudhary R N P and Mahapatra P K 2007 *Appl. Phys.* A **88** 217
[11] Sen S and Choudhary R N P 2007 *Appl. Phys.* A **87** 727
[12] Rouahi A, Kahouli A, Chalali F, Besland M P, Vallée C, Yangui B, Salimy S, Goullet A and Sylvestre A 2012 *J. Appl. Phys.* **112** 094104
[13] Wang W C *et al* 2011 *Thin Solid Films* **519** 5730
[14] Lukosius M, Baristiran-Kaynak C, Abrutis A, Skapas M, Kubilius V, Zaumer A, Ruhl G and Wenger Ch 2011 *Microelectron. Eng.* **88** 1529
[15] Chiang K C, Lai C H, Chin A (Senior Member, IEEE), Wang T J, Chiu H F, Chen J-R, McAlister S P (Senior Member, IEEE) and Chi C C 2005 *IEEE Electron Device Lett.* **26** 728

[16] Kremer F and Schönhals A (ed) 2003 *Broadband Dielectric Spectroscopy* (Berlin: Springer)
[17] Hammami H, Arous M, Lagache M and Kallel A 2007 *J. Alloys Compounds* **430** 1
[18] Rouahi A, Kahouli A, Sylvestre A and Yangui B 2012 *J. Alloys Compounds* **529** 84
[19] Gerhardt R 1994 *J. Phys. Chem. Solids* **55** 1491
[20] Jonscher A K 1999 *J. Phys. D: Appl. Phys.* **32** R57
[21] Kao K C 2004 *Dielectric Phenomena in Solids* (Amsterdam: Elsevier)
[22] Dutta A and Sinha T P 2006 *J. Phys. Chem. Solids* **67** 1484
[23] Yang C F 1996 *Jpn. J. Appl. Phys.* **35** 1806
[24] Viciosa M T, Dionisio M and Gomez Ribelles J L 2011 *Polymer* **52** 1944
[25] Ang C. and Yu Z. 2000 *Phys. Rev.* B **62** 228
[26] Wang C C and Zhang L W 2006 *Phys. Rev.* B **74** 024106